FRONTIERS OF PHYSICS

RESEARCH ARTICLE
Volume 21 / Issue 11 / 112202 / 2026

# Observation of an inelastic feshbach resonance between individual $^{87}$Rb and $^{39}$K atoms in optical tweezers

Kedi Wei[1], Shangjin Li[1], Ruike Wu[1], Yu Liu[1], Tao Chen[2,†], Bo Yan[1,‡]

1 Zhejiang Key Laboratory of Micro-nano Quantum Chips and Quantum Control, School of Physics, and State Key Laboratory for Extreme Photonics and Instrumentation, Zhejiang University, Hangzhou 310027, China
2 School of Physics, Xi'an Jiaotong University, Xi'an 710049, China
Corresponding authors. E-mail: †taochen@xjtu.edu.cn, ‡yanbohang@zju.edu.cn
Received January 6, 2026; accepted March 9, 2026



## ABSTRACT

An important route toward the preparation of cold molecules is magnetically tunable Feshbach resonances. Here we investigate an inelastic Feshbach resonance between a single pair of $^{87}$Rb and $^{39}$K atoms confined in an optical tweezer, with both atoms prepared in the $|F = 1, m_F = -1\rangle$ state. By developing an *in-situ* imaging scheme for $^{39}$K, we directly measure magnetic-field-dependent collisional loss without separating the atoms after the interaction. For weak confinement, the resonance position measured in our experiment differs from the bulk-gas experiments. In contrast, we observe a significant shift of the resonance toward higher magnetic fields as the tweezer trap depth increases. Coupled-channel calculations accounting for finite temperature effects fail to explain the magnitude of this shift, suggesting that it originates from differential optical responses of the open-channel atom pair and the weakly bound molecular state under strong confinement. Our results indicate that optical tweezer light can significantly modify Feshbach resonance properties, opening a pathway toward optical control of atom–atom interactions and weakly bound molecular states in dual-species tweezer platforms.

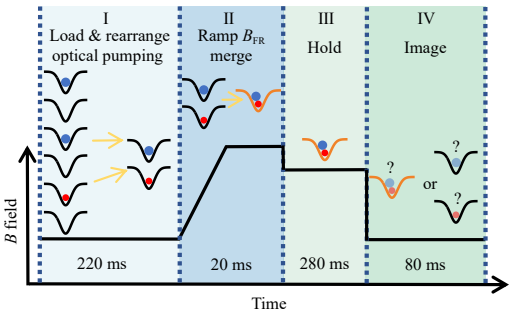


**Keywords** Feshbach resonance, ultracold molecule, dual species tweezer

## 1 Introduction

Cold molecules have been demonstrated to hold broad potential applications in quantum science and technology [1–3]. Precise control over their rich internal degrees of freedom and the tunability of the strong dipole–dipole interactions enable both the generation of high-fidelity quantum gates [4–6] and the quantum simulations of novel many-body phases of matter [7–11]. In addition, certain polar molecules have been exploited for precision measurements [12], e.g., searching for parity-violating weak interactions and the electron electric dipole moment [13–18]. One effective approach to creating cold molecules is using magnetic Feshbach resonance, i.e., associating two free atoms into a molecule by simply sweeping the magnetic field across the weakly-bound molecular states. Such externally controlled two-body scattering processes have been widely applied in bulk quantum gas experiments to generate bi-alkali molecular species [19], and recently extended to alkali-alkaline-earth(-like) systems [20–22]. Many theory frameworks, including the coupled-channel model and the multi-channel quantum defect theory, have been well developed to help interpret and understand these two-body scattering


https://doi.org/10.15302/frontphys.2026.112202

processes [23–31].

Optical tweezers provide a versatile platform with flexible tunabilities to study two-body and few-body collisions [32]. In contrast to bulk gas experiments, which generally require deep evaporative cooling to achieve sufficient density overlap, the tight confinement of optical tweezers naturally ensures high atomic densities suitable for investigating cold collisions. Also, we can study pure two-body scattering by preparing exactly two atoms in the same tight tweezer trap while completely eliminating many-body effects present in bulk gases, such as three-body loss and intraspecies scattering. To date, Feshbach resonances and the magneto-association of single diatomic molecules in optical tweezers have been demonstrated in a variety of systems, from early observations of confinement-induced resonance for two $^{6}$Li atoms [33] and the Feshbach loss spectroscopy of two $^{133}$Cs atoms [34] and a $^{87}$Rb$-^{133}$Cs atom pair [35], to the recent formation and precise coherent manipulations of single ground-state $^{87}$Rb$^{133}$Cs [36–38], $^{87}$Rb$^{85}$Rb [39, 40] and $^{23}$Na$^{133}$Cs [41–44] molecules.

Here we focus on the previously well investigated Rb$-$K system [45–51], but now in the context of optical tweezers. By preparing exactly two single $^{87}$Rb and $^{39}$K atoms in a tightly confining trap potential, we directly observe the magnetic-field-dependent inelastic collisional loss, with both initialized in the $|F=1, m_{\mathrm{F}}=-1\rangle$ Zeeman sublevels. For loss detection, we develop an *in-situ* image scheme for the $^{39}$K atom, which avoids the need to spatially separate the two atoms for independent detection after the collision stage, as is commonly done in previous Na$-$Cs [42] and Rb$-$Cs [35] tweezer experiments. Another point different from the above two cases [52, 53] is that the loss spectroscopy we observed exhibits a much stronger dependence on the tweezer trap potential, with the resonance positions significantly shifted by the strong tweezer confinement. This behavior also differs qualitatively from that observed in bulk gas experiments [48] and suggests the possibility of optically controlling Feshbach resonances.

To address the mechanism underlying this trap-depth-dependent shift of the resonance position, we employ coupled-channel calculations [24] to examine the effect of finite temperature on two free scattering atoms, without including light shifts of either the open-channel atom pair or the closed-channel molecular bound state. As the temperature-induced shifts predicted by this model remain far smaller than those observed experimentally, we suggest that the large shifts under strong tweezer confinement may originate from different optical responses of the open and closed channels. This interpretation, however, remains an open question and calls for further theoretical investigation, as the polarizabilities of weakly bound $^{87}$Rb$^{39}$K molecular states are not yet well characterized [54, 55]. Nevertheless, our experimental observations indicate that the optical tweezer light itself may be used to tune Feshbach resonances and control the energies of weakly bound molecular rovibrational states.

The paper is organized as follows. In Section 2, we describe our experimental details, mainly on the tweezer and magnetic field control, and how the *in-situ* image scheme works to detect the $^{39}$K atom loss. In Section 3, we show the loss spectroscopy by scanning the magnetic field at which the two-body scattering happens, and further characterize the dependence of the Feshbach resonance parameters on the tweezer trap depth. We also present a comparison between such a resonance position shift phenomenon and the predictions from the coupled-channel model. Finally, in Section 4, we give a brief summary and provide directions for further improvement and possible future directions in this dual-species tweezer platform.

## 2 Experimental methods

### 2.1 Tweezer loading and initial state preparation

The experiment is based on our previously reported dual-species optical tweezer setup [56, 57]. Cold $^{87}$Rb and $^{39}$K atomic ensembles are collected with a dual-species 3D magneto-optical trap (MOT), and further cooled via optical molasses. For $^{87}$Rb, we use the typical red molasses and achieve a temperature of $\sim 10(2)$ μK, while the $^{39}$K atoms are cooled down to $\sim 9(1)$ μK via the blue-detuned gray molasses. Then we simultaneously load the two species in a $1\times 6$ optical tweezer array generated by an acousto-optic deflector (AOD) using light at a frequency of 351.7 THz (locked to the Cs D2 line $|F=4\rangle \rightarrow |F'=5\rangle$ transition), resulting in a nearly uniform trap depth of $U_{\mathrm{Rb}}/k_{\mathrm{B}} = 780$ μK for $^{87}$Rb and $U_{\mathrm{K}}/k_{\mathrm{B}} = 560$ μK for $^{39}$K ($k_{\mathrm{B}}$ is the Boltzmann constant). The corresponding radial and axial trap frequencies, measured via parametric heating, are $2\pi\times 43(3)$, 3.40(5) kHz for $^{87}$Rb and $2\pi\times 56(4)$, 4.39(6) kHz for $^{39}$K, respectively. At these initial trap depths, the atomic temperatures measured using the release-and-recapture method are $T_{\mathrm{Rb}} = 32(6)$ μK and $T_{\mathrm{K}} = 35(13)$ μK respectively. The loading probabilities for the two species are approximately 0.5 each and are independent, with no observable crosstalk.

After loading, a first imaging step (not shown in Stage I of Fig. 1) is performed to identify occupied tweezers in the array. Imaging beams for both $^{87}$Rb and $^{39}$K atoms are applied simultaneously for a duration of 80 ms. For $^{87}$Rb, the 3D MOT beams are used for fluorescence imaging while simultaneously providing cooling to counteract fluorescence-induced heating. The cooling laser operates at an intensity of $\sim 1.1 I_{\mathrm{sat}}$ per beam, detuned by $-3.6$ MHz from the $F=2\rightarrow F'=3$ transition, while the repump laser is resonant to the $F=1\rightarrow F'=2$ transition with an intensity of $\sim 0.15 I_{\mathrm{sat}}$ for each beam. For

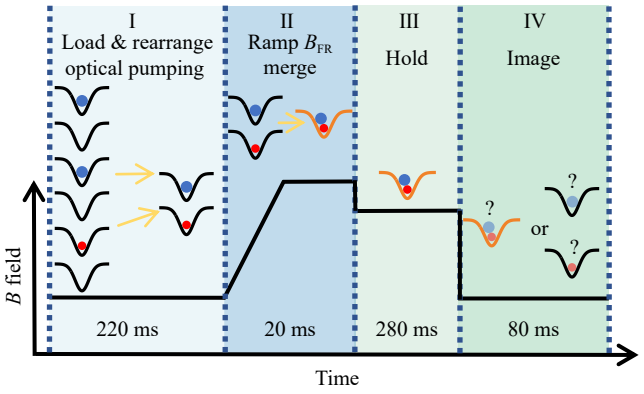


**Fig. 1** Experimental sequence for studying $^{87}$Rb–$^{39}$K two-body collisions in an optical tweezer. The sequence begins with probabilistic loading of an array of 850-nm optical tweezers, followed by rearrangement and optical pumping to deterministically prepare a single $^{87}$Rb–$^{39}$K atom pair in selected Zeeman sublevels (Stage I). Both atoms are then transferred into an auxiliary optical tweezer within 20 ms, during which the magnetic field is first ramped to a value of $B_{\mathrm{FR}}$, $\sim 16$ G higher than the subsequent hold field $B$, over the first 10 ms (Stage II). After a holding time of 280 ms at a specified magnetic field $B$ (Stage III), collisional loss of the atoms is detected using either the previously developed split-tweezer method or our *in-situ* $^{39}$K atom imaging technique, which does not require separating the two atoms into different tweezers (Stage IV). The orange trap indicates the auxiliary merged tweezer

$^{39}$K imaging, we use both $D_1$ and $D_2$ transitions [58, 59]. A relatively low-intensity $D_2$ MOT beam is applied for photon scattering, wherein the cooling laser is detuned by $+28.2$ MHz from the $F = 2 \rightarrow F' = 3$ transition and the repump component is detuned by $+33.7$ MHz from the $F = 1 \rightarrow F' = 2$ transition, both taking an intensity of $\sim 0.01 I_{\mathrm{sat}}$. At the same time, the 3D $D_1$ gray molasses cooling is applied to prevent atom loss due to fluorescence heating, with an intensity of $6 I_{\mathrm{sat}}$ per beam and the cooling-to-repump intensity ratio of $3:1$. The two-photon detuning is set to zero, and the single-photon detuning is $+46.2$ MHz relative to the $F = 2 \rightarrow F' = 2$ transition. Note that all detuning values quoted above do not include the tweezer-induced light shift. A prism is used to spatially separate the fluorescence signals of Rb and K on the camera, and the single atom imaging fidelity of 0.99 for $^{87}$Rb and 0.98 for $^{39}$K is achieved [56], respectively.

Finally, at the end of Stage I in Fig. 1, we perform rearrangement and optical pumping for initial state preparations. Empty tweezers are released, and two independent tweezers containing exactly one $^{87}$Rb atom and one $^{39}$K atom, respectively, are postselected. Owing to the relatively small size of our one-dimensional array, all possible rearrangement waveforms are exhaustively precomputed in advance [34, 60] and stored in the memory of an arbitrary waveform generator (Spectrum M4i.6631-x8). During the experimental sequence, appropriate waveforms are selected and output based on the initial loading configuration. Following a 2 ms rearrangement sequence, we achieve a deterministic loading probability of 96.8% for exactly one $^{87}$Rb atom and one $^{39}$K atom. Following the rearrangement, we optically pump both atoms to the $|F = 1, m_{\mathrm{F}} = -1\rangle$ state, with the preparation fidelities of 94(3)% for $^{87}$Rb and 88(2)% for $^{39}$K, respectively.

## 2.2 Trap merging and magnetic field control

Next, as shown in stage II in Fig. 1, we first ramp the magnetic field to $B_{\mathrm{FR}}$, $\sim 16$ G higher than the subsequent hold field $B$, over the first 10 ms, and then merge two single atoms into an auxiliary tweezer trap, within a duration of 20 ms. In general, the tweezer-merging process, which requires tuning the driving frequencies to bring the trap centers into spatial overlap, can induce significant parametric heating and lead to substantial atom loss [61, 62]. To mitigate heating-induced loss, we introduce a stationary auxiliary tweezer whose trapping laser frequency is detuned by approximately 100 MHz from that of the main tweezer array. With this configuration, each loaded tweezer can independently overlap with the auxiliary trap, thereby avoiding low-frequency beating between trap lasers. In contrast, we observe strong atom loss when directly merging two loaded tweezers originating from the same laser source, due to their mutual interference in the frequency domain, which generates low-frequency beat notes on the kilohertz scale and induces parametric heating as the traps approach spatial overlap.

Our merging procedure has two steps. First, the auxiliary tweezer is overlapped with one of the loaded tweezers, and the atom is transferred into the auxiliary trap by adiabatically turning off the original tweezer. The same procedure is then repeated for the second loaded tweezer. During the merging process, it is essential to balance the trap depths of the participating tweezers to minimize atomic heating. When properly optimized, the merging operation becomes nearly lossless and fully reversible, allowing the atom pair to be separated back into individual tweezers for detection.

The overlap density of the $^{87}$Rb $-^{39}$K atom pair in the merged optical tweezer is determined by [63, 64]

$$\bar{n}_2 = \left( \frac{1}{2\pi k_{\mathrm{B}}} \frac{m_{\mathrm{Rb}} \bar{\omega}_{\mathrm{Rb}}^2}{T_{\mathrm{K}}/\beta^2 + T_{\mathrm{Rb}}} \right)^{3/2}, \tag{1}$$

where the relation $m_{\mathrm{K}} \omega_{\mathrm{K}}^2 = \beta^2 m_{\mathrm{Rb}} \omega_{\mathrm{Rb}}^2$ holds, and $k_{\mathrm{B}}$ is the Boltzmann constant, $m_{\mathrm{Rb}}$ and $m_{\mathrm{K}}$ are Rb and K atom masses, respectively. $T_{\mathrm{Rb}}$ and $T_{\mathrm{K}}$ denote the temperatures of the Rb and K in the optical tweezer. The geometric mean trap frequency is defined as $\bar{\omega} = (\omega_x \omega_y \omega_z)^{1/3}$, where $\omega_{x,y,z}$ are the trap frequencies along three spatial axes.

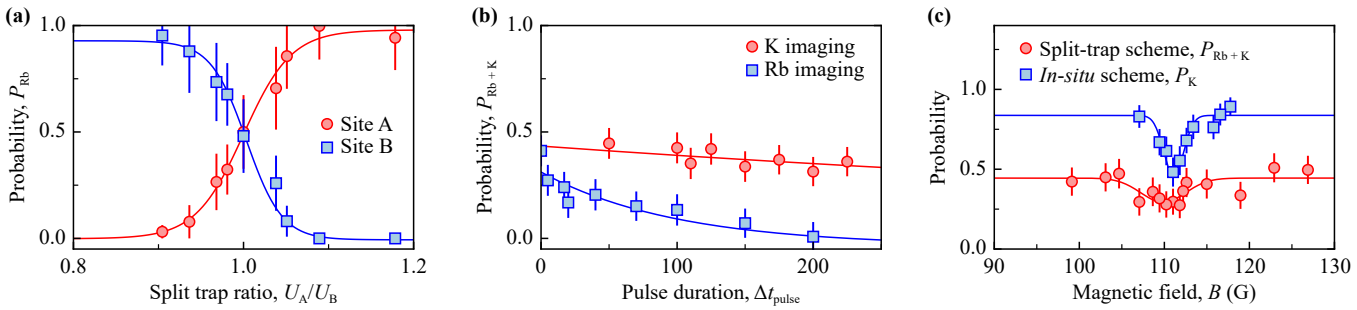


**Fig. 2** **(a)** Atomic re-allocation probabilities in two split tweezers with different trap-depth ratios. In the experiment, we first confirm the presence of a single Rb atom in the tweezer before initiating the splitting procedure. The splitting procedure is as follows: Site B (the fixed auxiliary tweezer) is ramped on within 3 ms to a trap depth of $U_{Rb}/k_B = 550\,\mu K$ for $^{87}Rb$. Subsequently, the trap depth of Site A (the movable tweezer controlled by an AOD) is ramped to a value $U_A$. Site A is then translated over a distance of $12\,\mu m$ relative to Site B within 0.5 ms to spatially separate the two tweezers. After splitting, the trap depths of both Site A and Site B are ramped back to $U_{Rb}/k_B = 780\,\mu K$ for $^{87}Rb$ for imaging, and the probability $P_{Rb}$ of finding a Rb atom in each of the two sites is measured. The trap-depth ratio during splitting varies by changing the trap depth $U_A$. The solid curves are Boltzmann fits to the experimental data. **(b)** Effect of Rb (red circles) and K (blue squares) imaging light on the survival of Rb–K atom pairs in the auxiliary merged tweezer. The experimental sequence follows Fig. 1, except that no Feshbach magnetic field is applied during Stage III. During the hold time, either Rb or K imaging light is applied to the atom pair for a duration $\Delta t_{pulse}$. The survival probability of the Rb–K pair, $P_{Rb+K}$, is then measured using the split-trap detection method. Solid curves are exponential fits to the data. The fit yields a characteristic time constant of $\tau_K = 867(171)$ ms for the K imaging light, while for the Rb imaging light we have $\tau_{Rb} = 99(53)$ ms. **(c)** Comparison of Feshbach resonance spectra obtained using the split-trap detection scheme (red circles) and the *in-situ* K detection scheme (blue squares). In the latter scheme, only the survival probability of the K atom is monitored. Its reliability is confirmed by the results in Fig. 2(b), which show that the K imaging light introduces negligible additional two-body loss within the imaging duration of 80 ms. The *in-situ* K detection scheme yields a significantly improved signal-to-noise ratio. Solid curves are Gaussian fits to the respective data sets.

Using these parameters, we calculate the mean overlap density as $\bar{n}_2 = 1.5 \times 10^{11}\,cm^{-3}$ at a trap depth of $U_{Rb}/k_B \approx 780\,\mu K$. This value is lower than that for other two-species tweezer experiments [34, 42], which primarily arises from the relatively large waist of our optical tweezer, measured to be $2.1(2)\,\mu m$. Additionally, we note that the atoms are not prepared in the motional ground state in this work. Nevertheless, the tweezer-based platform offers an alternative approach for studying interactions in systems where achieving high densities in bulk gases is challenging.

After merging, we suddenly tune the magnetic field to a specific static value $B$, which is held for a duration of $\sim 280$ ms to enable sufficient atomic collisions; see stage III in Fig. 1. Finally, the magnetic field is rapidly ramped back to zero (stage IV in Fig. 1), and we perform fluorescence imaging again to confirm the remaining atomic fraction that gives the collisional loss under each specific magnetic field.

### 2.3 *In-situ* detection of atom loss

In the final detection stage IV in Fig. 1, two methods are employed for atom loss detection. One is the conventional split-trap imaging used in previous experiments [34, 42, 65], another is the direct *in-situ* detection of remaining $^{39}K$ atom fractions in the auxiliary tweezer after the collisions. For the split-trap detection, atom pairs are separated back into two individual tweezers, labelled as $A$ and $B$, by reversing the last step in the previous merging procedure, following which two $\sim 80$ ms imaging pulses (with the same parameters as those for the first imaging pulses in stage I) are applied for $^{87}Rb$ and $^{39}K$ atoms to determine their populations respectively. During the splitting, it is important to make the tweezers $A$ and $B$ take nearly an identical trap depth to ensure an equal probability of the atomic re-allocation. As shown in Fig. 2(a), we verify this point by measuring the $^{87}Rb$ fractions $P_{Rb}$ in each trap after splitting. We set the trap-depth ratio close to 1 when measuring the joint probability, $P_{Rb+K}$, for simultaneously detecting one $^{87}Rb$ atom in one split tweezer trap and one $^{39}K$ atom in another.

While the joint probability $P_{Rb+K}$, having an upper bound of 0.5, provides direct information of the survival rate of an atom pair, it is sensitive to the trap-depth ratio of the two split tweezer traps and requires two imaging pulses that degrade signal-to-noise ratios. To improve the quality of the loss spectroscopy, we have developed an *in-situ* detection scheme, in which the $^{39}K$ imaging pulse is applied directly to the atom pair in the merged auxiliary tweezer, without performing the splitting operation. This approach relies on the fact that the in-situ imaging pulse does not significantly disturb the atom pair on the $\sim$80 ms imaging timescale. We measure the survival probability of $^{39}K$ atoms, denoted

as $P_{\mathrm{K}}$, which completely eliminates the influence of the splitting process and requires only a single imaging shot. As a result, the signal-to-noise ratio of the loss spectroscopy is significantly improved.

Now let us move to the demonstration of how such an *in-situ* imaging scheme works for our Rb−K system. We first experimentally examine the influence of the imaging light on the atom pair. During the hold time, we apply either $^{87}$Rb or $^{39}$K imaging light (see Section 2.1) with different pulse durations $\Delta t_{\mathrm{pulse}}$, and subsequently use the split-trap detection method to resolve the atom pair's joint survival probability $P_{\mathrm{Rb+K}}$. Figure 2(b) shows the measured $P_{\mathrm{Rb+K}}$ as a function of $\Delta t_{\mathrm{pulse}}$. Exponential fits to the two sets of data reveal that the lifetime of the atom pair under the exposure of $^{39}$K ($^{87}$Rb) imaging light is $\tau_{\mathrm{K}} = 867(171)$ ms ($\tau_{\mathrm{Rb}} = 99(53)$ ms). We attribute this phenomenon to the photoassociation induced by the red-detuned $^{87}$Rb imaging light, while the blue-detuned light used for $^{39}$K imaging should not support such a photoassociation process [66]. The immunity of the atom pair to the $^{39}$K imaging light, evidenced by $\tau_{\mathrm{K}}$ being much longer than the imaging pulse duration, motivates us to perform *in-situ* detection by just recording the loss of $^{39}$K atom after the collisional event happens. The key advantage of this method is that it does not rely on the balance ratio of the splitting tweezers and thus is more robust against the experimental imperfections and noise.

## 3 Results and discussion

### 3.1 Feshbach loss spectroscopy

Figure 2(c) shows the dependences of the measured atom loss on the holding magnetic field (see stage III in Fig. 1), using the above two different detection schemes, respectively. Here we let the merged tweezer trap depth $U_{\mathrm{Rb}}/k_{\mathrm{B}} \approx 780\ \mu$K (corresponding to a tweezer intensity of 162 kW/cm$^2$) for $^{87}$Rb to benchmark the two-body inelastic collisions. For two atoms both in the $|F = 1, m_{\mathrm{F}} = -1\rangle$ states, the split-trap imaging detection gives a loss dip at $B_{\mathrm{res}} = 109.9(7)$ G from a Gaussian fit to the measured data, with the full width at half maximum of $\sim 6(2)$ G. As a comparison, the *in-situ* detection of solely $^{39}$K atom shows the resonance position lies at $B_{\mathrm{res}} = 110.5(2)$ G with a width of $\sim 3.1(5)$ G. The two results are consistent with each other within the experimental uncertainties, but it is clear that the latter *in-situ* method achieves better signal-to-noise ratio and dip contrast. In our subsequent experiments, we therefore use the *in-situ* method to locate the Feshbach resonance positions under different merged trap depths.

At a tweezer intensity of 162 kW/cm$^2$, the resonance position measured in our experiment differs from the bulk-gas value of $B_{\mathrm{res}} = 117.6(4)$ G reported for $^{87}$Rb and $^{39}$K atoms both prepared in the $|F = 1, m_{\mathrm{F}} = -1\rangle$ state [48] by approximately 7 G, a deviation that significantly exceeds our experimental uncertainty. We attribute this discrepancy most likely to the fact that the atoms are not prepared in the motional ground state of the optical tweezer. Note that the width of the dip extracted from the Gaussian fit does not necessarily match the width of

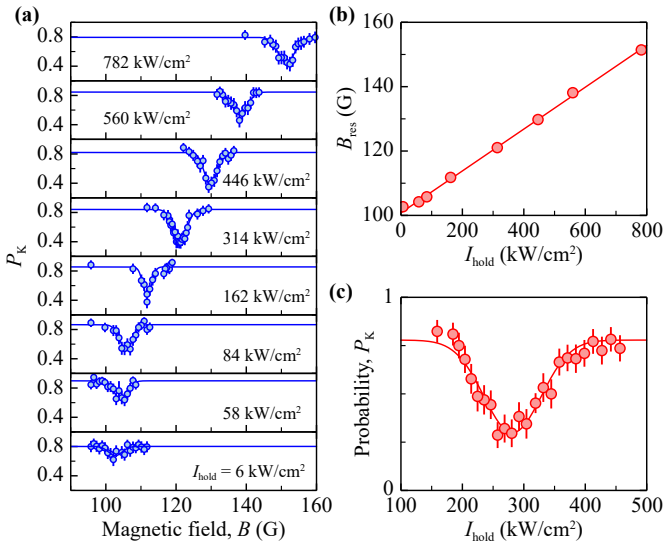


**Fig. 3** Effect of optical tweezer trap on the observed $^{87}$Rb–$^{39}$K Feshbach resonance. **(a)** Measured Feshbach resonance spectra at different optical tweezer powers. In the experiment, after the merge (Stage II in Fig. 1), the power of the tweezer containing a Rb–K atom pair (the orange tweezer in Fig. 1) is ramped to a target value $I_{\mathrm{hold}}$ within 5 ms, following which two-body collisions happen and the *in-situ* imaging detections are performed (Stages III and IV). From bottom to top, the strength of $I_{\mathrm{hold}}$ increases from $\sim 6$ kW/cm$^2$ to $\sim 782$ kW/cm$^2$, where the upper limit is constrained to the total available laser power in our setup. The magnetic field is calibrated by probing the Zeeman splitting of the $^{87}$Rb $|F = 2, m_{\mathrm{F}} = +2\rangle \rightarrow |F' = 3, m'_{\mathrm{F}} = +3\rangle$ transition at both high and low fields, followed by a linear fit. This calibration yields a magnetic field uncertainty below 0.5 G across the entire range of trap depths used in the experiment. This uncertainty is incorporated into the Gaussian fitting procedure for the loss spectra, and the final uncertainties in $B_{\mathrm{res}}$ are given by the standard errors of these fits. The resulting field uncertainty is estimated to be below 1%. **(b)** Extracted resonance magnetic field positions, $B_{\mathrm{res}}$, as a function of the optical tweezer power $I_{\mathrm{hold}}$, from the measured spectra in (a). A linear fit (solid line) yields a slope of $\sim 0.065(1)$ G/(kW/cm$^2$). **(c)** Dependence of the Feshbach resonance induced loss probability on the optical tweezer intensity at a fixed magnetic field of $\sim 117$ G. The experimental sequence is identical to that in (a), except that the magnetic field during the hold stage (Stage III) is maintained at $\sim 117$ G while $I_{\mathrm{hold}}$ is varied after the merge stage. With a Gaussian fit (solid line), the resonance dip is located at $I_{\mathrm{hold}} = 282(3)$ kW/cm$^2$, with a full width at half maximum of 110(9) kW/cm$^2$. Error bars in (a) and (c) indicate the standard errors from multiple repeated experimental data sets, while those in (b) are errors of the fitting parameters.

the Feshbach resonance (measured to be $\sim 1.3$ G, cf. Ref. [48]), as the two quantities are defined differently.

Based on the above benchmark, we further explore the influence of the tweezer confinement on the Feshbach resonance by varying the collisional trap depth during Stage III in Fig. 1. Since the trap depth definition depends on atomic species, here we use the laser intensity $I_{\rm hold}$ to characterize the tweezer confinement strength. Figure 3(a) presents a series of measured loss spectroscopy with the *in-situ* detection scheme, under different tweezer trap intensities. By increasing the intensity from $\sim 6\ \mathrm{kW/cm^2}$ to $\sim 782\ \mathrm{kW/cm^2}$, corresponding to the trap depth $U_{\rm Rb}/k_{\rm B}$ increasing from $\sim 31\ \mu$K to $\sim 3760\ \mu$K, the resonance position moves from $\sim 102.7(4)$ G to $\sim 151.4(2)$ G. In Fig. 3(b), we summarize the resonance positions $B_{\rm res}$ as a function of the trap intensity $I_{\rm hold}$. Overall, the resonance position exhibits an approximately linear dependence on the tweezer confinement. A linear fit yields a slope of $\sim 0.065(1)\ \mathrm{G/(kW/cm^2)}$. We note that this value is much larger than those observed in other platforms, e.g., less than $0.001\ \mathrm{G/(kW/cm^2)}$ for Na−Cs system [52] and on the order of $\sim 0.01\ \mathrm{G/(kW/cm^2)}$ for Rb−Cs system [53]. Section 3.2 will give more discussions on this significant shift.

The pronounced trap-depth dependence observed here suggests a potential protocol of controlling magnetic Feshbach resonances using optical confinement. To demonstrate this capability, we fix the magnetic field and examine the sensitivity of the two-body inelastic loss to the tweezer intensity $I_{\rm hold}$. As shown in Fig. 3(c), for $B$ field at $\sim 117$ G, the resonance dip is located at $I_{\rm hold} = 282(3)\ \mathrm{kW/cm^2}$. This result indicates that the optical potential alone can be used to modify the two-body inelastic collision rate. Compared with magnetic-field sweeps, optical control enables faster ramping speeds, spatially localized tuning, and potentially lower technical noise. This mechanism differs from conventional optical Feshbach resonances [67–69], which rely on near-resonant light to couple colliding atoms to excited molecular states and typically suffer from strong heating losses. In contrast, the tweezer light used here is far detuned from atomic resonances, thereby avoiding significant heating, even compared with two-photon Raman-based optical Feshbach schemes. Moreover, in tweezer platforms, additional tightly focused beams could be used to locally switch on and off two-body loss or molecular association, offering further flexibility based on our observations.

### 3.2 Discussion on the trap-dependent shift

Two factors associated with the change of the trap depth can affect the properties of the Feshbach resonance: the temperature of the two atoms and the strong light shifts of the relevant open and closed scattering channels. To identify which effect dominates the pronounced shift of the resonance position, we perform coupled-channel scattering calculations to examine the dependence on atomic temperature. Since coupled-channel models have been widely used to address scattering problems in a variety of experimental systems [70–73], supported by well-developed numerical packages [74], we provide only a brief outline here.

The Hamiltonian for an interacting Rb–K atom pair under tight tweezer confinements reads

$$H = \frac{\hbar^2}{2\mu}\left(-\frac{1}{r}\frac{\partial^2}{\partial r^2}r + \frac{\hat{L}^2}{r^2}\right) + H_{\rm Rb} + H_{\rm K} + V(r) + U_{\rm RbK}(r, I), \tag{2}$$

where $\mu$ is the reduced mass of the atom pair, and $\hat{L}$ indicates the rotational angular momentum operator. The single atom Hamiltonians $H_{\rm Rb}$ and $H_{\rm K}$ include the hyperfine couplings, magnetic $B$ field dependent Zeeman couplings. The interaction operator $V(r)$ is determined by the two interatomic potentials of both the $X^1\Sigma$ singlet and $a^3\Sigma$ triplet states for the RbK molecule. Here we use the calibrated potential parameters based on multiple precise molecular spectroscopy in Ref. [75]. The additional input $U_{\rm RbK}(r, I)$ accounts for the tweezer-induced light shift to the bound state of the diatomic molecule and should depend on the interatomic distance $r$ according to Ref. [76]. Note that when $r \to \infty$, $U_{\rm RbK}(r, I)$ should equal the total Stark shift of two individual $^{87}$Rb and $^{39}$K atoms under the tweezer confinement.

We first benchmark our calculations by considering zero-energy two-body scattering, neglecting both finite-temperature effects and tweezer-induced light shifts. Figure 4(a) shows the absolute energy $E_{\rm in}$ of the entrance channel $\mathrm{Rb}\,|F = 1, m_{\rm F} = -1\rangle + \mathrm{K}\,|F = 1, m_{\rm F} = -1\rangle$ under different magnetic field strengths, by diagonalizing the single atom Hamiltonian $H_{\rm Rb} + H_{\rm K}$. We locate the bound state distribution for each $B$ field value using a similar propagating method to that described in Refs. [25, 77]. As shown in Fig. 4(b), the energy difference between the molecular bound state and the entrance channel, $E_{\rm bound} - E_{\rm in}$, crosses zero at $\sim 111.3$ G where the Feshbach resonance occurs. We further calculate the $s$-wave scattering length $a_s$ as a function of magnetic field $B$; see Fig. 4(c). We obtain the resonance position at $B_{\rm res} = 111.3$ G with the width $\Delta = -1.5$ G, in agreement with both previous experimental observations and our measured loss spectroscopy under a low tweezer trap depth [Fig. 2(c)].

Next we check the temperature effect. Different from the Na–Cs and Rb–Cs cases where the trapping effect can be directly input into the theory model (see Ref. [36]) as both atoms stay in the ground $n = 0$ state of the trap potential, the effect of the trapping state occupation (For a trap depth of $U_{\rm Rb}/k_{\rm B} = 777\ \mu$K, the mean occupation numbers are $\bar{n} \approx 14$ for Rb and $\bar{n} \approx 4$ for K) in our experiment is treated as an averaged finite temperature effect in our scattering calculations. The two atomic

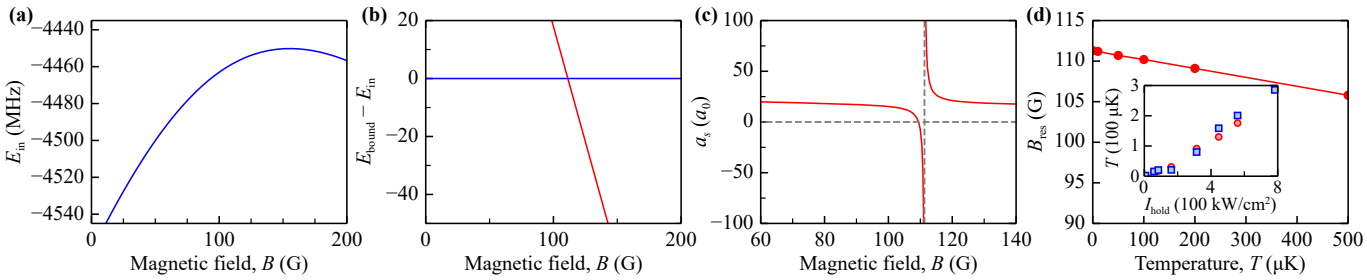


**Fig. 4** Predictions of the low-field Feshbach resonance for $^{87}$Rb−$^{39}$K atom pair with both in the $|F=1, m_F=-1\rangle$ states from the coupled-channel calculations. **(a)** Absolute energy $E_{in}$ for the entrance channel $^{87}\text{Rb}\,|F=1, m_F=-1\rangle + ^{39}|F=1, m_F=-1\rangle$ under different magnetic field strengths. **(b)** Calculated energy differences between the weakly bound molecular state and the entrance channel energy (red line), within the range $[-50, 20]$ MHz, under low magnetic field. The blue line indicates the entrance channel energy as a reference to clearly show the sharp slope for the Feshbach resonance that occurs at the cross point $B_{res} \sim 111.3$ G. This is calculated with the coupled-channel model, without considering the temperature effect and the tweezer confinement. **(c)** Calculated zero-energy $s$-wave scattering length $a_s$ vs. the magnetic field $B$ around the resonance position $B_{res} \sim 111.3$ G (vertical dashed line). The width of this resonance is $\Delta \sim -1.5$ G, which is determined by the cross point with the zero horizontal dashed line. **(d)** Dependence of the resonance position $B_{res}$ on the initial temperature of the atom pair. The coupled-channel calculation shows a linear variation of the positions versus the increase of the temperature. The inset figure shows the measured single atom temperatures for both $^{87}$Rb (blue squares) and $^{39}$K (red circles), ranging from several μK to $\sim 300$ μK under different tweezer light intensities.

species have different temperatures at different tweezer trap depths in our experiment. As shown in the inset of Fig. 4(d), the atomic temperature ranges from $\sim 1.7$ μK to $\sim 300$ μK when the tweezer confinement moves from weak to strong in our experiment. The coupled-channel calculations with the initial temperature (that determines the collisional energy) as an input show that the resonance positions shift to smaller $B$ field values compared to the zero-energy case. As illustrated in Fig. 4(d), the shift shows a linear behavior versus the temperature change, but in opposite direction to our experimental observations [Fig. 3(b)].

We therefore conclude that the large resonance shifts observed under strong tweezer confinement are most likely caused by differential light shifts between the open entrance channel and the closed-channel molecular bound state. For the red-detuned trapping light at $\sim 852$ nm in our $^{87}$Rb–$^{39}$K platform, multiple molecular transitions, from the closed-channel weakly-bound vibrational state in $(5S+4S)$ electronic manifold, to the deep vibrational states held in upper excited $(5P+4S)$ and $(5S+4P)$ electronic potentials, should largely contribute to the polarizability value $\alpha_{RbK}$ here. At present, however, only the polarizability of the absolute rovibrational ground state of the RbK molecule has been measured [55], while the Stark shifts and the possible $r$-dependent polarizability of weakly bound molecular states remain unknown. Based on our experimental data, here we can provide an estimation of the polarizability of the weakly-bound molecular state by assuming it is $r$-independent and letting $U_{RbK} \propto \alpha_{RbK} I$. With the trap depth calibration for both atoms, $U_{Rb}$ and $U_K$, and the calculated slope of the energy difference between the open and closed channels, $k_E/h = -1.7$ MHz/$G$, we have $\alpha_{RbK} = 2(U_{Rb} + U_K + k_E B)/I \approx h \times 28 \times 10^{-5}$ MHz/(W/cm$^2$) from the experimental data points measured in Fig. 3. This value is on the same order of magnitude as that for the rovibrational ground state in Ref. [55]. Although our calculations qualitatively indicate that the observed resonance shifts originate from the optical response to strong tweezer confinement, a quantitative description of this effect remains an open problem and is left for future investigation.

## 4 Conclusion and outlook

In summary, we have observed an inelastic Feshbach resonance between $^{87}$Rb and $^{39}$K atoms, with both in the $|F=1, m_F=-1\rangle$ state, in an optical tweezer. To achieve improved detection performance, we developed an *in-situ* imaging scheme for our Rb–K platform, which enables a systematic study of the dependence of Feshbach loss spectroscopy on the tweezer confinement strength. At a tweezer intensity of 162 kW/cm$^2$, the resonance position measured in our experiment differs from the bulk-gas experiments. In contrast to other systems, such as Na–Cs and Rb–Cs, we observe that the resonance position shifts significantly toward higher magnetic fields as the tweezer confinement becomes stronger. Our coupled-channel analysis shows that this behavior cannot be explained by temperature variations associated with different trap depths. We therefore attribute the observed shift to differential optical responses between the free scattering atoms and the weakly bound molecular states, an effect that remains an open question and warrants further investigation.

Looking forward, we plan to implement Raman sideband

cooling to prepare both atomic species in the motional ground state of the optical tweezer [53, 78]. Achieving full motional control is a key prerequisite for the efficient and coherent formation of Feshbach molecules and will enable a more quantitative investigation of how the resonance properties depend on the initial motional states and collision energy. In combination with precise control of the tweezer confinement, this will allow us to explore confinement-induced modifications of scattering processes beyond the thermal regime. Moreover, as demonstrated in the Rb–Cs system [53], the differential polarizability responsible for the resonance shift may exhibit a significant dependence on the trapping wavelength; a systematic study of this wavelength dependence in our Rb–K system is an interesting direction for future work. More broadly, the dual-species optical tweezer platform provides a versatile setting for studying few-body physics with an exact and well-defined particle number. Possible future directions include investigations of three- and four-body collisions, atom–molecule and molecule–molecule interactions, and the role of confinement and light-induced shifts in these processes, based on flexible precise control over both the magnetic field and the optical response.

**Declarations** The authors declare that they have no competing interests and there are no conflicts.

**Acknowledgements** We acknowledge support from the National Key Research and Development Program of China under Grant Nos. 2023YFA1406703 and 2022YFA1404203, the Quantum Science and Technology-National Science and Technology Major Project under Grant No. 2024ZD0300601, the National Natural Science Foundation of China under Grant Nos. 92576201, 12425408, and U21A20437, and the Fundamental Research Funds for the Central Universities under Grant No. 2024FZZX02-01-02.

## References

1. S. A. Moses, J. P. Covey, M. T. Miecnikowski, D. S. Jin, and J. Ye, New frontiers for quantum gases of polar molecules, *Nat. Phys.* 13(1), 13 (2017)
2. S. L. Cornish, M. R. Tarbutt, and K. R. Hazzard, Quantum computation and quantum simulation with ultracold molecules, *Nat. Phys.* 20(5), 730 (2024)
3. T. Langen, G. Valtolina, D. Wang, and J. Ye, Quantum state manipulation and cooling of ultracold molecules, *Nat. Phys.* 20(5), 702 (2024)
4. P. D. Gregory, J. A. Blackmore, S. L. Bromley, J. M. Hutson, and S. L. Cornish, Robust storage qubits in ultracold polar molecules, *Nat. Phys.* 17(10), 1149 (2021)
5. C. M. Holland, Y. Lu, and L. W. Cheuk, On-demand entanglement of molecules in a reconfigurable optical tweezer array, *Science* 382(6675), 1143 (2023)
6. L. R. Picard, A. J. Park, G. E. Patenotte, S. Gebretsadkan, D. Wellnitz, A. M. Rey, and K. K. Ni, Entanglement and iSWAP gate between molecular qubits, *Nature* 637(8047), 821 (2025)
7. A. V. Gorshkov, S. R. Manmana, G. Chen, E. Demler, M. D. Lukin, and A. M. Rey, Quantum magnetism with polar alkali-metal dimers, *Phys. Rev. A* 84(3), 033619 (2011)
8. B. Yan, S. A. Moses, B. Gadway, J. P. Covey, K. R. A. Hazzard, A. M. Rey, D. S. Jin, and J. Ye, Observation of dipolar spin-exchange interactions with lattice-confined polar molecules, *Nature* 501(7468), 521 (2013)
9. N. Y. Yao, M. P. Zaletel, D. M. Stamper-Kurn, and A. Vishwanath, A quantum dipolar spin liquid, *Nat. Phys.* 14(4), 405 (2018)
10. B. Sundar, B. Gadway, and K. R. Hazzard, Synthetic dimensions in ultracold polar molecules, *Sci. Rep.* 8, 3422 (2018)
11. A. N. Carroll, H. Hirzler, C. Miller, D. Wellnitz, S. R. Muleady, J. Lin, K. P. Zamarski, R. R. Wang, J. L. Bohn, A. M. Rey, and J. Ye, Observation of generalized *t-J* spin dynamics with tunable dipolar interactions, *Science* 388(6745), 381 (2025)
12. D. DeMille, N. R. Hutzler, A. M. Rey, and T. Zelevinsky, Quantum sensing and metrology for fundamental physics with molecules, *Nat. Phys.* 20(5), 741 (2024)
13. A. Collaboration, Improved limit on the electric dipole moment of the electron, *Nature* 562(7727), 355 (2018)
14. J. Lim, J. R. Almond, M. A. Trigatzis, J. A. Devlin, N. J. Fitch, B. E. Sauer, M. R. Tarbutt, and E. A. Hinds, Laser cooled YbF molecules for measuring the electron's electric dipole moment, *Phys. Rev. Lett.* 120(12), 123201 (2018)
15. T. S. Roussy, L. Caldwell, T. Wright, W. B. Cairncross, Y. Shagam, K. B. Ng, N. Schlossberger, S. Y. Park, A. Wang, J. Ye, and E. A. Cornell, An improved bound on the electron's electric dipole moment, *Science* 381(6653), 46 (2023)
16. L. Anderegg, N. B. Vilas, C. Hallas, P. Robichaud, A. Jadbabaie, J. M. Doyle, and N. R. Hutzler, Quantum control of trapped polyatomic molecules for eEDM searches, *Science* 382(6671), 665 (2023)
17. Z. Zeng, S. Deng, S. Yang, and B. Yan, Three-dimensional magneto-optical trapping of barium monofluoride, *Phys. Rev. Lett.* 133(14), 143404 (2024)
18. W. Bu, Y. Zhang, Q. Liang, T. Chen, and B. Yan, Saturated absorption spectroscopy of buffer-gas-cooled Barium monofluoride molecules, *Front. Phys. (Beijing)* 17(6), 62502 (2022)
19. C. Chin, R. Grimm, P. Julienne, and E. Tiesinga, Feshbach resonances in ultracold gases, *Rev. Mod. Phys.* 82(2), 1225 (2010)
20. V. Barbé, A. Ciamei, B. Pasquiou, L. Reichsöllner, F. Schreck, P. S. Żuchowski, and J. M. Hutson, Observation of Feshbach resonances between alkali and closed-shell atoms, *Nat. Phys.* 14(9), 881 (2018)
21. B. C. Yang, M. D. Frye, A. Guttridge, J. Aldegunde, P. S. Żuchowski, S. L. Cornish, and J. M. Hutson, Magnetic Feshbach resonances in ultracold collisions between Cs and Yb atoms, *Phys. Rev. A* 100(2), 022704 (2019)
22. W. Dowd, R. J. Roy, R. K. Shrestha, A. Petrov, C. Makrides, S. Kotochigova, and S. Gupta, Magnetic field

dependent interactions in an ultracold Li–Yb($^3P_2$) mixture, *New J. Phys.* 17(5), 055007 (2015)
23. R. Stock, I. H. Deutsch, and E. L. Bolda, Quantum state control via trap-induced shape resonance in ultracold atomic collisions, *Phys. Rev. Lett.* 91(18), 183201 (2003)
24. J. M. Hutson, E. Tiesinga, and P. S. Julienne, Avoided crossings between bound states of ultracold cesium dimers, *Phys. Rev. A* 78(5), 052703 (2008)
25. M. Berninger, A. Zenesini, B. Huang, W. Harm, H. C. Nägerl, F. Ferlaino, R. Grimm, P. S. Julienne, and J. M. Hutson, Feshbach resonances, weakly bound molecular states, and coupled-channel potentials for cesium at high magnetic fields, *Phys. Rev. A* 87(3), 032517 (2013)
26. J. D. Hood, Y. Yu, Y. W. Lin, J. T. Zhang, K. Wang, L. R. Liu, B. Gao, and K. K. Ni, Multichannel interactions of two atoms in an optical tweezer, *Phys. Rev. Res.* 2(2), 023108 (2020)
27. B. Gao, E. Tiesinga, C. J. Williams, and P. S. Julienne, Multichannel quantum-defect theory for slow atomic collisions, *Phys. Rev. A* 72(4), 042719 (2005)
28. C. Makrides and B. Gao, Multichannel quantum-defect theory for magnetic Feshbach resonances in heteronuclear group-I systems, *Phys. Rev. A* 89(6), 062718 (2014)
29. B. Gao, Multichannel quantum-defect theory for anisotropic interactions, arXiv: 2008.08018 (2020)
30. J. Liu and B. Liu, Molecule production via Feshbach resonance in bosonic systems, *Front. Phys. China* 5(2), 123 (2010)
31. X. Zhang, X. Hu, D. Wang, X. Liu, and W. Liu, Dynamics of Bose-Einstein condensates near Feshbach resonance in external potential, *Front. Phys. (Beijing)* 6(1), 46 (2011)
32. A. M. Kaufman and K. K. Ni, Quantum science with optical tweezer arrays of ultracold atoms and molecules, *Nat. Phys.* 17(12), 1324 (2021)
33. S. Sala, G. Zürn, T. Lompe, A. N. Wenz, S. Murmann, F. Serwane, S. Jochim, and A. Saenz, Coherent molecule formation in anharmonic potentials near confinement-induced resonances, *Phys. Rev. Lett.* 110(20), 203202 (2013)
34. R. V. Brooks, A. Guttridge, M. D. Frye, D. K. Ruttley, S. Spence, J. M. Hutson, and S. L. Cornish, Feshbach spectroscopy of Cs atom pairs in optical tweezers, *New J. Phys.* 24(11), 113051 (2022)
35. R. Brooks, V, S. Spence, A. Guttridge, A. Alampounti, A. Rakonjac, L. A. McArd, J. M. Hutson, and S. L. Cornish, Preparation of one $^{87}$Rb and one $^{133}$Cs atom in a single optical tweezer, *New J. Phys.* 23, 065002 (2021)
36. D. K. Ruttley, A. Guttridge, S. Spence, R. C. Bird, C. R. Le Sueur, J. M. Hutson, and S. L. Cornish, Formation of ultracold molecules by merging optical tweezers, *Phys. Rev. Lett.* 130(22), 223401 (2023)
37. D. K. Ruttley, A. Guttridge, T. R. Hepworth, and S. L. Cornish, Enhanced quantum control of individual ultracold molecules using optical tweezer arrays, *PRX Quantum* 5(2), 020333 (2024)
38. D. K. Ruttley, T. R. Hepworth, A. Guttridge, and S. L. Cornish, Long-lived entanglement of molecules in magic-wavelength optical tweezers, *Nature* 637(8047), 827 (2025)
39. P. Xu, J. Yang, M. Liu, X. He, Y. Zeng, K. Wang, J. Wang, D. Papoular, G. Shlyapnikov, and M. Zhan, Interaction-induced decay of a heteronuclear two-atom system, *Nat. Commun.* 6(1), 7803 (2015)
40. X. He, K. Wang, J. Zhuang, P. Xu, X. Gao, R. Guo, C. Sheng, M. Liu, J. Wang, J. Li, G. V. Shlyapnikov, and M. Zhan, Coherently forming a single molecule in an optical trap, *Science* 370(6514), 331 (2020)
41. L. R. Liu, J. D. Hood, Y. Yu, J. T. Zhang, K. Wang, Y. W. Lin, T. Rosenband, and K. K. Ni, Molecular assembly of ground-state cooled single atoms, *Phys. Rev. X* 9(2), 021039 (2019)
42. J. T. Zhang, Y. Yu, W. B. Cairncross, K. Wang, L. R. B. Picard, J. D. Hood, Y. W. Lin, J. M. Hutson, and K. K. Ni, Forming a single molecule by magnetoassociation in an optical tweezer, *Phys. Rev. Lett.* 124(25), 253401 (2020)
43. Y. Yu, K. Wang, J. D. Hood, L. R. B. Picard, J. T. Zhang, W. B. Cairncross, J. M. Hutson, R. Gonzalez-Ferez, T. Rosenband, and K. K. Ni, Coherent optical creation of a single molecule, *Phys. Rev. X* 11(3), 031061 (2021)
44. W. B. Cairncross, J. T. Zhang, L. R. B. Picard, Y. Yu, K. Wang, and K. K. Ni, Assembly of a rovibrational ground state molecule in an optical tweezer, *Phys. Rev. Lett.* 126(12), 123402 (2021)
45. K. K. Ni, S. Ospelkaus, M. De Miranda, A. Pe'Er, B. Neyenhuis, J. Zirbel, S. Kotochigova, P. Julienne, D. Jin, and J. Ye, A high phase-space-density gas of polar molecules, *Science* 322(5899), 231 (2008)
46. P. S. Julienne, Ultracold molecules from ultracold atoms: A case study with the KRb molecule, *Faraday Discuss.* 142, 361 (2009)
47. S. Kotochigova, E. Tiesinga, and P. S. Julienne, Multichannel modelling of the formation of vibrationally cold polar KRb molecules, *New J. Phys.* 11(5), 055043 (2009)
48. A. Simoni, M. Zaccanti, C. D'Errico, M. Fattori, G. Roati, M. Inguscio, and G. Modugno, Near-threshold model for ultracold KRb dimers from interisotope Feshbach spectroscopy, *Phys. Rev. A* 77(5), 052705 (2008)
49. C. Klempt, T. Henninger, O. Topic, J. Will, W. Ertmer, E. Tiemann, and J. Arlt, $^{40}$K–$^{87}$Rb Feshbach resonances: Modeling the interatomic potential, *Phys. Rev. A* 76(2), 020701 (2007)
50. P. Wang, Z. Fu, S. Chai, and J. Zhang, Feshbach resonances in an ultracold mixture of $^{87}$Rb and $^{40}$K, *Chin. Phys. B* 20(10), 103401 (2011)
51. C. Mi, K. S. Nawaz, P. Wang, L. Chen, Z. Meng, L. Huang, and J. Zhang, Production of dual species Bose–Einstein condensates of $^{39}$K and $^{87}$Rb, *Chin. Phys. B* 30(6), 063401 (2021)
52. J. Zhang, Assembling an array of polar molecules with full quantum-state control, Ph. D. thesis, Harvard University, 2021
53. S. Spence, Assembling single RbCs molecules with optical tweezers, Ph. D. thesis, Durham University, 2023
54. J. Aldegunde, B. A. Rivington, P. S. Żuchowski, and J. M. Hutson, Hyperfine energy levels of alkali-metal dimers: Ground-state polar molecules in electric and magnetic fields, *Phys. Rev. A* 78(3), 033434 (2008)
55. B. Neyenhuis, B. Yan, S. A. Moses, J. P. Covey, A.

Chotia, A. Petrov, S. Kotochigova, J. Ye, and D. S. Jin, Anisotropic polarizability of ultracold polar $^{40}$K $^{87}$Rb molecules, *Phys. Rev. Lett.* 109(23), 230403 (2012)
56. Y. Wei, K. Wei, S. Li, and B. Yan, Dual-species optical tweezer for Rb and K atoms, *Phys. Rev. A* 110(4), 043118 (2024)
57. K. Wei, Y. Wei, S. Li, and B. Yan, Compact dual MOT apparatus of K and Rb for optical tweezer experiment, *Chin. Phys. B* 35(1), 013701 (2026)
58. J. Ang'ong'a, C. Huang, J. P. Covey, and B. Gadway, Gray molasses cooling of $^{39}$K atoms in optical tweezers, *Phys. Rev. Res.* 4(1), 013240 (2022)
59. T. Chen, C. Huang, I. Velkovsky, K. R. Hazzard, J. P. Covey, and B. Gadway, Strongly interacting Rydberg atoms in synthetic dimensions with a magnetic flux, *Nat. Commun.* 15(1), 2675 (2024)
60. W. Tian, W. J. Wee, A. Qu, B. J. M. Lim, P. R. Datla, V. P. W. Koh, and H. Loh, Parallel Assembly of Arbitrary Defect-Free Atom Arrays with a Multitweezer Algorithm, *Phys. Rev. Appl.* 19(3), 034048 (2023)
61. T. A. Savard, K. M. O'Hara, and J. E. Thomas, Laser-noise-induced heating in far-off resonance optical traps, *Phys. Rev. A* 56(2), R1095 (1997)
62. H. J. Levine, Quantum information processing and quantum simulation with programmable Rydberg atom arrays, Ph.D. Thesis, Harvard University, Cambridge, Massachusetts, 2021
63. A. Guttridge, S. A. Hopkins, S. L. Kemp, M. D. Frye, J. M. Hutson, and S. L. Cornish, Interspecies thermalization in an ultracold mixture of Cs and Yb in an optical trap, *Phys. Rev. A* 96(1), 012704 (2017)
64. M. Anderlini, D. Ciampini, D. Cossart, E. Courtade, M. Cristiani, C. Sias, O. Morsch, and E. Arimondo, Model for collisions in ultracold-atom mixtures, *Phys. Rev. A* 72(3), 033408 (2005)
65. K. Wang, X. He, R. Guo, P. Xu, C. Sheng, J. Zhuang, Z. Xiong, M. Liu, J. Wang, and M. Zhan, Preparation of a heteronuclear two-atom system in the three-dimensional ground state in an optical tweezer, *Phys. Rev. A* 100(6), 063429 (2019)
66. M. Weyland, S. S. Szigeti, R. A. B. Hobbs, P. Ruksasakchai, L. Sanchez, and M. F. Andersen, Pair correlations and photoassociation dynamics of two atoms in an optical tweezer, *Phys. Rev. Lett.* 126(8), 083401 (2021)
67. M. Theis, G. Thalhammer, K. Winkler, M. Hellwig, G. Ruff, R. Grimm, and J. H. Denschlag, Tuning the scattering length with an optically induced Feshbach resonance, *Phys. Rev. Lett.* 93(12), 123001 (2004)
68. G. Thalhammer, M. Theis, K. Winkler, R. Grimm, and J. H. Denschlag, Inducing an optical Feshbach resonance via stimulated Raman coupling, *Phys. Rev. A* 71(3), 033403 (2005)
69. T. L. Nicholson, S. Blatt, B. J. Bloom, J. R. Williams, J. W. Thomsen, J. Ye, and P. S. Julienne, Optical Feshbach resonances: Field-dressed theory and comparison with experiments, *Phys. Rev. A* 92(2), 022709 (2015)
70. M. D. Frye, B. C. Yang, and J. M. Hutson, Ultracold collisions of Cs atoms in excited Zeeman and hyperfine states, *Phys. Rev. A* 100(2), 022702 (2019)
71. A. Petrov, C. Makrides, and S. Kotochigova, Magnetic control of ultra-cold $^{6}$Li and $^{174}$Yb($^{3}$P$_2$) atom mixtures with Feshbach resonances, *New J. Phys.* 17(4), 045010 (2015)
72. T. Chen, C. Zhang, X. Li, J. Qian, and Y. Wang, Anisotropy induced Feshbach resonances in mixture of $^{6}$Li($^{2}$S)+$^{171}$Yb($^{3}$P$_2$), *New J. Phys.* 17(10), 103036 (2015)
73. M. L. González-Martínez and J. M. Hutson, Magnetically tunable Feshbach resonances in Li + Yb($^{3}$P$_J$), *Phys. Rev. A* 88(2), 020701 (2013)
74. J. M. Hutson and C. R. Le Sueur, molscat: A program for non-reactive quantum scattering calculations on atomic and molecular collisions, *Comput. Phys. Commun.* 241, 9 (2019)
75. A. Pashov, O. Docenko, M. Tamanis, R. Ferber, H. Knöckel, and E. Tiemann, Coupling of the $X^1\Sigma^+$ and $a^3\Sigma^+$ states of KRb, *Phys. Rev. A* 76(2), 022511 (2007)
76. M. Tomza, R. González-Férez, C. P. Koch, and R. Moszynski, Controlling magnetic Feshbach resonances in polar open-shell molecules with nonresonant light, *Phys. Rev. Lett.* 112(11), 113201 (2014)
77. M. D. Frye and J. M. Hutson, Characterizing Feshbach resonances in ultracold scattering calculations, *Phys. Rev. A* 96(4), 042705 (2017)
78. Y. Yu, N. R. Hutzler, J. T. Zhang, L. R. Liu, J. D. Hood, T. Rosenband, and K. K. Ni, Motional-ground-state cooling outside the Lamb-Dicke regime, *Phys. Rev. A* 97(6), 063423 (2018)